Volume 27
Number 7
21 February 2025
Pages 881–1046

CrystEngComm

rsc.li/crystengcomm

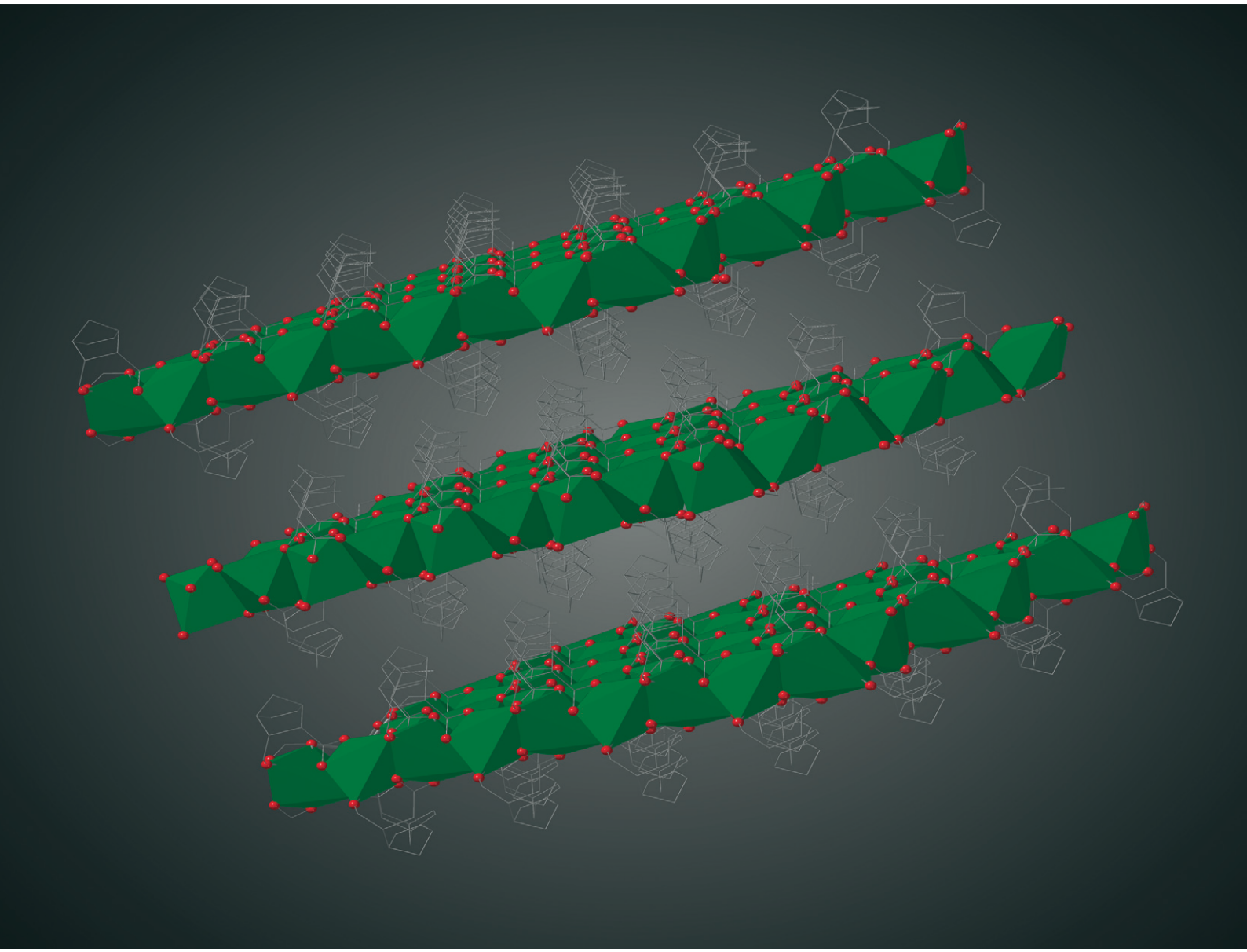

ISSN 1466-8033

ROYAL SOCIETY OF CHEMISTRY

PAPER

Abdul Malik P. Peedikakkal *et al.*
Blue- and white-light emitting 2D metal–organic frameworks of *cis*-5-norbornene-*endo*-2,3-dicarboxylic acid

CrystEngComm

ROYAL SOCIETY OF CHEMISTRY

PAPER

View Article Online
View Journal | View Issue

Cite this: *CrystEngComm*, 2025, **27**, 913

Blue- and white-light emitting 2D metal–organic frameworks of *cis*-5-norbornene-*endo*-2,3-dicarboxylic acid†

Ahmed Mohammed A. Alghamdi,[a] Shakeeba Cholikadam,[a] Mohammed Fettouhi,[ab] Abdul Nasar Kalanthoden,[a] Almaz S. Jalilov*[c] and Abdul Malik P. Peedikakkal *[ab]

Two-dimensional (2D) materials have recently gained increased attention owing to their potential applications in catalysis and as luminescent materials in optoelectronics. Herein, we report the synthesis of two distinct blue- and white-light emitting crystalline 2D-metal organic frameworks (MOFs) using *cis*-5-norbornene-*endo*-2,3-dicarboxylic acid (NDA) as a ligand with $Pb(NO_3)_2$ [Pb(NDA)] (**1**) and $Zn(OAc)_2{\cdot}2H_2O$ [Zn(NDA)] (**2**), respectively. Compound **1** forms *hepta*-coordinated Pb(II) geometry with greater distortion, resulting in a 2D MOF with a (4,4) network topology. In contrast, in **2**, Zn(II) centers are linked through NDA ligands to furnish a 2D MOF. The final structural characteristics of the synthesized compounds were significantly impacted by the carboxylic acid ligand. Upon excitation at 365 nm, compound **2** displayed blue-light emission, while compound **1** demonstrated near-white-light emission of solid-state photoluminescence (PL). The differing emissions of the two 2D sheets were associated with the bridging NDA ligand and the relative structural differences between the 2D structures. The shortest non-bonded metal-to-metal distance is lower in **1** than that in **2**. Compound **1** exhibits a higher packing efficiency of bridging-metal centered clusters of layers; such packing is less pronounced in compound **2** because of the differences in coordination geometries. These differences profoundly affect the luminescent characteristics of **1** and **2**.

Received 27th September 2024,
Accepted 7th January 2025

DOI: 10.1039/d4ce00985a

rsc.li/crystengcomm

Introduction

Luminescent metal–organic frameworks (MOFs) have gained significant consideration owing to their simple synthesis, biomedical imaging properties, versatile design capabilities, luminescent functional sites, nonlinear optics, fluorescence recognition, and high practical value in lighting and displays.[1–5] Recently, many synthetic efforts have focused on synthesizing numerous luminescent MOFs using lanthanides, transition metals, and main group metals.[5,6] These materials offer tunable luminescence properties, including white-light emitting features.[7] Among these approaches, the use of white-light-emitting materials is a highly engaged subject in luminescent MOF studies.[7,8] Nevertheless, the emission of many inorganic and organic luminescent compounds is limited to a specific portion of the visible spectrum. The majority of white-light emission materials have been synthesized using methods that involve the combination of monochromatic emissions.[9] To create materials that emit white light, it is essential to employ straightforward methods for efficiently adjusting and managing emission colours.[10] Currently, the fabrication of white light devices mostly relies on the integration of multiple components utilizing either the RGB (red, green, and blue) three-color or YB (yellow, blue) two-color mixing concepts.[11] However, these white-light emitting materials (WLEMs) consisting of many components commonly encounter issues such as color imbalance and instability due to the varying degradation rates of each luminescent component and challenges in managing energy transmission.[11] Investigations are ongoing to address these issues, and relevant findings have been reported for various materials, such as organic molecules, coordination polymers, nanomaterials, and others.[12] Single-component WLEM systems are more advantageous than multicomponent systems owing to their ease of reproduction and simple preparation. However, effectively managing the appropriate

[a] *Department of Chemistry, King Fahd University of Petroleum and Minerals, Dhahran 31261, Saudi Arabia. E-mail: abdulmalik@kfupm.edu.sa*
[b] *Interdisciplinary Research Center for Refining and Advanced Chemicals, King Fahd University of Petroleum and Minerals, Dhahran 31261, Saudi Arabia*
[c] *Department of Biology, Chemistry and Environmental Sciences, American University of Sharjah, P.O. Box 26666, Sharjah, United Arab Emirates. E-mail: ajalilov@aus.edu*

† Electronic supplementary information (ESI) available. CCDC 2356413 and 2356409 contain the supplementary crystallographic data for **1** and **2**, respectively, including X-ray powder patterns, FT-IR spectra, TGA data and solid-state UV-vis spectra. For ESI and crystallographic data in CIF or other electronic format see DOI: **https://doi.org/10.1039/d4ce00985a**

blending of various emission centers in multicomponent systems remains a difficult task.[13,14] Because of the availability of a wide range of organic and inorganic small molecules, it is possible to create organic–inorganic hybrid metal halides (OIMHs) with specific crystal architectures.[15] These OIMHs can be adjusted in terms of their molecular size and possess unique photovoltaic properties. Another notable feature is color tuning, which is achieved by adjusting temperature and has potential applications in temperature measuring.[16] Moreover, they enhanced the quality of light in their preferred lighting products by incorporating high-performance near-UV LED 365 nm phosphor-converted LEDs. Fan *et al.*[17] successfully synthesized an organic–inorganic hybrid structure that exhibits adjustable emission ranging from orange-red to blue. This tunability is achieved by varying the Pb/Sn metal ratio or adjusting the excitation laser. They successfully achieved white-light emission and a remarkable photoluminescence (PL) quantum yield of 39%.

Two-dimensional (2D) MOFs hold significant potential in various applications.[18] However, there are still difficulties in creating stable materials with consistent synthesis methods and comprehending the exact relationships between synthesis factors and material properties. Hence, the development of robust and highly efficient 2D MOFs for optical devices holds immense importance. Currently, persistent efforts have been devoted to attaining a future that involves the use of exceptionally effective electroluminescent (EL) materials.[19] Among the many types of luminescent MOFs, Zn(II) MOFs are particularly fascinating on account of their unique properties.[20] These metal ions exhibit various geometries and coordination numbers, and they form various architectures, resulting in the emission of vibrant blue light.[20] Pb(II) exhibits lone pair effects, which contribute to its tendency to bind various ligands.[21] This unique characteristic of Pb(II) plays a crucial role in its structural modulation and white-light emission.[21] Consequently, its exceptional properties enable both control and modulation. Furthermore, in this system, the interaction between the ligand and metal can result in ligand-to-metal (LMCT) or metal-to-ligand charge transfer (MLCT). The spherical (*s*) and principal (*p*) orbitals of the Pb(II) center involved in these transitions can cause the emission of light across a wide range of wavelengths in Pb(II) based MOFs. Interactions between Pb(II) orbitals can contribute to the construction of broad-spectrum emission in Pb(II) MOFs.[22,23] The synthesis of 2D lead-MOFs was achieved by incorporating boron-imidazolate ligands with deformable Pb(II) halide units.[24] This study indicates that this 2D MOF demonstrates exceptional ability in generating white light. Efforts to develop blue light-emitting materials with wide band gaps[25] have been ongoing for a considerable period. However, to successfully create full-color organic light emitting diodes (OLEDs), it is necessary to address concerns regarding the efficiency and lifespan of blue emitting materials. The primary focus of this extensive study is on the advancement of blue luminescent materials, primarily utilizing aromatic chemical molecules and organic polymers.[26] Furthermore, the careful selection of ligands[27] is essential in creating new MOFs because of their numerous coordination modes, which meet the geometric requirements of metal centres to build attractive structural designs.[28] The isomeric form of (±)*endo*,*exo*-5-norbornene-2,3-dicarboxylic acid has been known to act as a ligand in several metal complexes and MOFs.[29] Although several coordination networks have been explored, the *cis*-5-norbornene-*endo*-2,3-dicarboxylic acid (NDA) with Pb(II) and Zn(II) have been unexplored. The steric influence and stereochemistry of the ligand force the formation of 2D networks. The selection of NDA as a ligand is especially important because of its specific geometries and steric arrangement, which enable the construction of 2D MOFs. Owing to strong steric demand that is inherent in NDA, it is possible to achieve proper chelation and bridging of metal centers that are fundamental in the formation of a 2D network topology. This rigidity in coordination together with the special stereochemistry of the ligand leads to the formation of 2D networks because there is relatively low torsional strain and thus high energy for formation of a metal-to-ligand bond.[30] In addition, it has been proved that the flexibility of NDA to assume specific coordination modes contributes to the dimensionality of the resulting frameworks, which suggests that understanding ligands is crucial for predicting the structure of the final MOFs.[31,32] Two MOFs were obtained through the reaction of Pb(II) and Zn(II) ions with the NDA ligand. These MOFs are denoted as [Pb(NDA)](**1**) and [Zn(NDA)](**2**). Compound **1** was synthesized by reacting $Pb(NO_3)_2$ with NDA dissolved in DMF, while compound **2** was synthesized through the reaction between $Zn(OAc)_2{\cdot}2H_2O$ and NDA, which was dissolved in water. Compounds **1** and **2** exhibited a 2D sheet-like structure, which was formed through the combined chelating and bridging modes of NDA. Compound **1** demonstrates PL that emits near white light, while compound **2** emits blue light when excited at a wavelength of 365 nm. The details of our investigation are given below.

Experimental section

Materials and methods

All precursors were commercially obtained and used without further purification. All solvents used were reagent grade. The yield of compounds **1** and **2** was measured using the metal salts $Pb(NO_3)_2$ and $Zn(OAc)_2{\cdot}2H_2O$. A PXRD pattern was obtained using a Rigaku Ultima IV X-ray diffractometer. Thermogravimetric analysis (TGA) of **1** and **2** was performed using an SDT 2960 TGA thermal analyzer. Samples were heated to 800 °C at a rate of 5 °C min^{-1} under a nitrogen flow of 50 mL min^{-1}. FT-IR spectra were obtained using KBr pellets (NICOLET iS10 FT-IR). Solid-state UV-visible spectra were collected at ambient temperature using a UV-3600

Shimadzu UV-visible spectrometer equipped with an incorporating sphere and barium sulphate reflecting reference. Room temperature steady-state PL measurements and time-dependent PL measurements were recorded using a Hamamatsu Quantaurus-Tau Fluorescence lifetime spectrometer. All of the solid-state spectra for a crystalline powder of **1** and **2** were recorded at ambient conditions using glass pellets as sample holders.

Caution! *Lead compounds are potentially toxic and must be utilized in limited amounts and treated carefully.*

Synthesis of Pb-MOFs [Pb(NDA)] (1)

A solution containing NDA (12 mg, 0.07 mmol) and $Pb(NO_3)_2$ (23 mg, 0.07 mmol) diluted in 2 mL of DMF was subjected to heating at 80 °C for 24 h in a closed vial. Colorless block-like crystals of **1** were produced after 2 days. After filtration, crystals were obtained and subsequently dried in a desiccator. Yield: 22 mg (81%). Anal. calcd. for $PbC_9H_8O_4{\cdot}1.95H_2O$: C, 25.59; H, 2.84; found: C, 25.09; H, 2.29; selected IR (KBr, cm^{-1}): 3507(w), 2976(w), 1632(m), 1557(s), 1532(s), 1397(s), 1272(m), and 1235(m). Thermal gravimetric analysis (H_2O weight loss %) calcd. 4.44%; found 5.28%.

Synthesis of Zn-MOFs [Zn(NDA)] (2)

A mixture containing $Zn(OAc)_2{\cdot}2H_2O$ (26 mg, 0.12 mmol) and NDA (12 mg, 0.07 mmol) dissolved in 2 mL of distilled water was heated at 80 °C for 24 h in a sealed vial. Colorless block-like crystals of **2** were obtained after 2 days. The crystals were obtained through filtration and subsequently dried in a desiccator. Yield: 6.6 mg (22%). Anal. calcd. for $ZnC_9H_8O_4{\cdot}1H_2O$: C, 41.02; H, 3.82; found: C, 41.69; H, 3.92; selected IR (KBr, cm^{-1}): 3655(s), 2966(s), 1592(m), 1525(s), 1432(s), 1305(m), 847(s), and 734(s).

Single crystal X-ray crystallographic analysis

The single crystal X-ray analysis of compounds **1** and **2** were obtained using a Bruker APEX II CCD diffractometer. Graphite-monochromated MoKα radiation with a wavelength of 0.71073 Å was used in the diffractometer together with a sealed tube with a power output of 2.4 kW. SADABS[33] was utilized to perform absorption corrections, while the crystallographic suite SHELXTL[34] was employed for calculations. The Flack parameter for the non-centrosymmetric Pb structure was refined to 0.16(3), confirming that the absolute structure is correctly defined by atomic coordinates. Crystallographic data, along with details of data collection and modification for compounds **1** and **2**, are outlined in Table 1.

Table 1 Crystallographic data for **1** and **2**

Compounds	**1**	**2**
Crystal system	Orthorhombic	Monoclinic
Empirical formula	$C_9H_8O_4Pb$	$C_9H_8O_4Zn$
Formula weight	387.34	245.52
Temperature/K	299(2)	299(2)
Space group	*Iba*2	$P2_1/c$
a/Å	8.7725(6)	11.2667(5)
b/Å	23.311(2)	9.0284(4)
c/Å	8.6198(6)	9.2720(4)
α/°	90	90
β/°	90	107.830(2)
γ/°	90	90
Volume/Å^3	1762.7(2)	897.74(8)
Z	8	4
ρ, Mg cm^{-3}	2.919	1.816
μ/mm^{-1}	19.124	9.208
refln collected	37 026	24 073
Independent reflns/R_{int}/GoF	2240/0.0863/0.942	2634/0.0531/0.935
Final $R[I > 2\sigma(I)]$, R_1/wR_2	0.0310/0.0715	0.0443/0.1235

Results and discussion

Synthesis and characterization

Compound [Pb(NDA)] (**1**) was synthesized by reacting $Pb(NO_3)_2$ with NDA in a DMF solution. After 48 h of heating, colorless block-like crystals were produced. Compound [Zn(NDA)] (**2**) was synthesized as colorless block-shaped crystals within two days by reacting NDA with $Zn(OAc)_2{\cdot}2H_2O$ in water. The final topology of the MOFs is affected by crystallization conditions and the presence of carboxylate anions.[35] The as-synthesized crystals of compounds **1** and **2** were studied using powder X-ray diffraction studies (Fig. S6 and S7†). The PXRD patterns of the as-synthesized samples closely matched the simulated patterns from crystallographic data, showing the formation of highly pure compounds. FT-IR spectra of both compounds were determined (as shown in Fig. S8 and S9†).

Thermogravimetric analysis (TGA) was conducted on compounds **1** and **2** (Fig. S10 and S11†). The initial weight loss in compound **1** indicates the loss of adsorbed water molecules, which is consistent with elemental analysis. Thereafter, the compound started to decompose as the temperature increased to 300 °C. Compound **2** remains stable up to 400 °C, as shown in Fig. S11.†

The FT-IR spectrum of compound **1** (Fig. S8†) shows asymmetric stretching vibration of the carboxylate group at 1632 cm^{-1}, with a symmetric stretching at 1397 cm^{-1}. The difference between these values ($\Delta\nu = \nu_{asym} - \nu_{sym}$) is 235 cm^{-1}, suggesting that the carboxylate ligand is coordinated to Pb(II) in a bidentate manner. Similarly, in compound **2** (Fig. S9†), carboxylate group asymmetric stretching is observed at 1592 cm^{-1}, and symmetric stretching at 1334 cm^{-1}, with a $\Delta\nu$ of 258 cm^{-1}, also indicating bidentate coordination to Zn(II).

Crystal structures of compounds 1 and 2

Single crystal X-ray structural analysis was investigated for compound **1**, which shows that the compound crystallized in an orthorhombic system with $Z = 8$ in the space group *Iba*2. The fundamental unit of **1** is displayed in Fig. S1.† Pb(II) has a significantly distorted heptacoordinated

geometry, with a stereochemically active lone pair at the Pb(II) metal center, as shown in Fig. S2 and S3.† The stereochemically active lone pair on Pb(II) plays an essential role in shaping the structure, adding a unique distortion that leads to the formation of a non-centrosymmetric framework. The carboxylate of NDA strongly coordinated to the Pb(1) atoms through chelating and bridging coordination modes [Pb(1)–O(1), 2.551(1) Å; Pb(1)–O(2), 2.503(8) Å; Pb(1)–O(3), 2.405(8) Å; Pb(1)–O(4), 2.619(1) Å]. Furthermore, the combination of Pb(1) with the NDA ligand results in the construction of metal bridged clusters consisting of [Pb(O_2CC–)] along the *ac* plane, as shown in Fig. 1a. This, in turn, leads to the construction of a 2D MOF with a four-connected topology, as depicted in Fig. 1b–d. However, the 2D frameworks exhibit slightly corrugated layers of (4,4)-networks when the Pb(1) metal atoms connected. The average non-bonded distance between the two adjacent Pb(1) atoms is 4.4 Å, as shown in the Fig. 1c. There are two non-bonded distances between the opposite Pb(1) atoms, measuring 5.5 Å and 6.9 Å, as shown in Fig. 1c. The interlayer distance between the two layers is 10.7 Å, as shown in Fig. 1d.

Compound **2** forms crystals in the $P2_1/c$ space group within a monoclinic system, with $Z = 4$. The fundamental unit of **1** is displayed in Fig. S3.† Zn(II) metal centers exhibit tetrahedral geometry, with two carboxylates acting as bridges. The Zn(1) ion coordinates with the carboxylate oxygen atoms of the NDA ligand [Zn(1)–O(2), 1.939(2) Å; Zn(1)–O(1), 1.980(2) Å; Zn(1)–O(3), 1.967(2) Å; Zn(1)–O(4), 1.961(2) Å]. NDA connects to three Zn(II) metal centers using two carboxylate ligands, as shown in Fig. 2a. This connectivity results in the formation of a 2D sheet with a (4,4) network topology, as displayed in Fig. 2b. In contrast, no corrugated layers are present in **2** as we observed in **1**. The average non-bonded shortest metal-to-metal distance is 4.6 Å in a single layer, as shown in Fig. 2b. The average non-bonded distances between the two opposite metal centers are 5.3–6.7 Å, as shown in Fig. 2b. The shortest interlayer distance between the two layers is 11.2 Å. The shortest non-bonded metal–metal distances are larger in **2** in comparison to that in **1**. The interlayer distances in **2** are also found to be higher than those in **1**. Furthermore, the packing efficiency of bridged-metal centered clusters is higher in **1** in comparison to that in **2**, as observed in Fig. 1c and 2c. The highest BFDH relative area is 0.194 along the (020) face in **1** compared with the highest relative area of 0.179 along the (100) face in **2**.

Optical properties

Chemical sensors, electroluminescent displays, and photochemistry are among the few potential applications of compounds **1** and **2** owing to their photoluminescent properties. Herein, the PL of **1** and **2** was confirmed

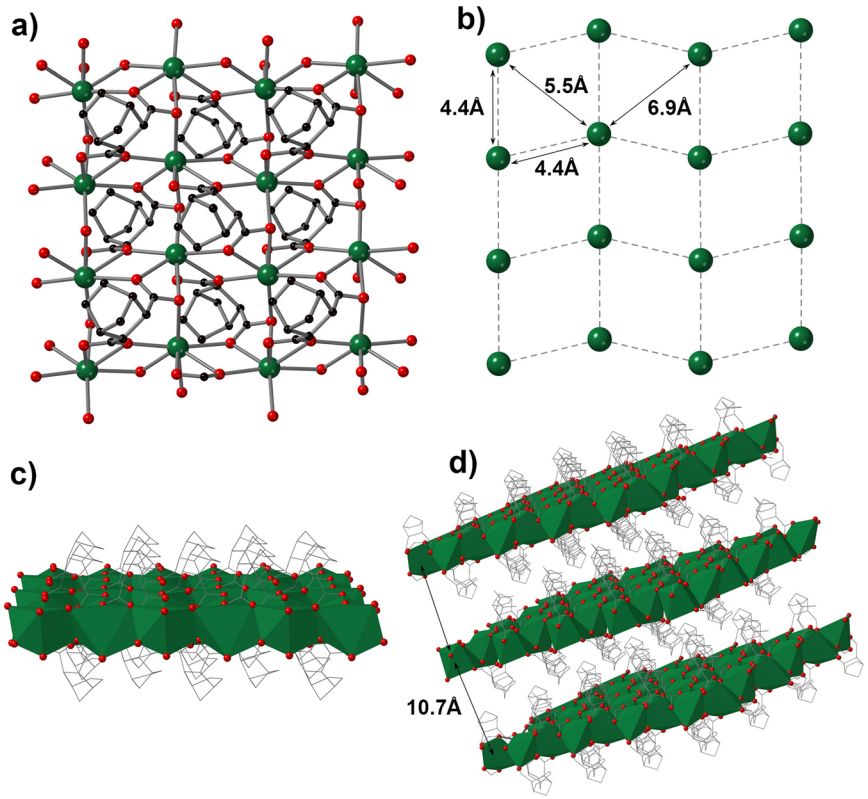

Fig. 1 (a) A portion of the 2D sheet structure of **1**. (b) Illustration of the (4,4) network topology in **1** with various metal-to-metal distances. (c) Perspective view of the single 2D layer. (d) Perspective view of the three 2D layers in **1**. The distance between the two adjacent layers is 10.7 Å.

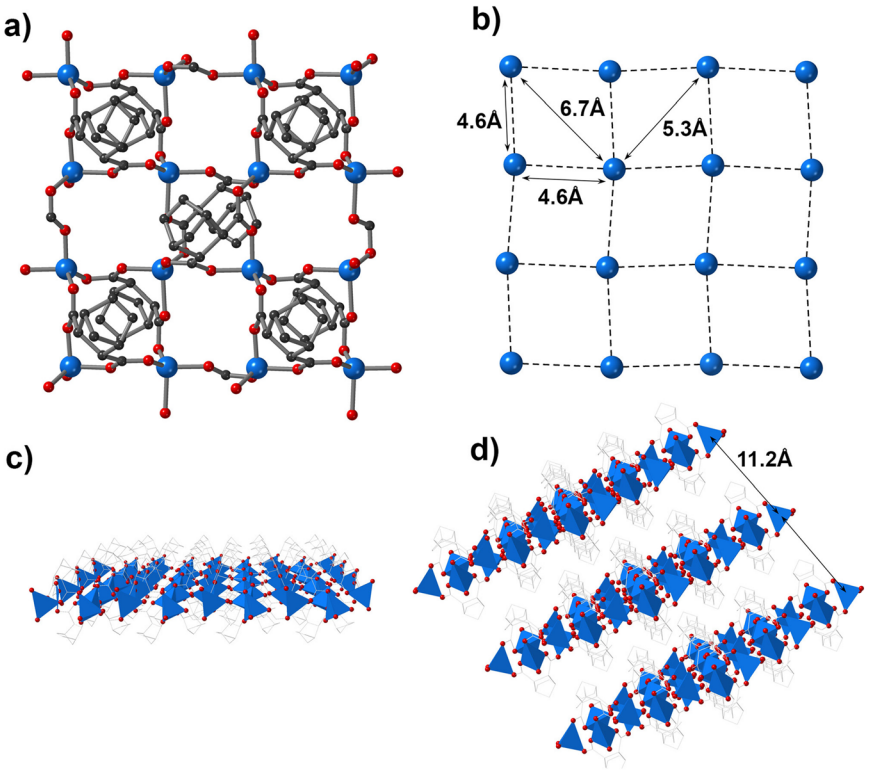

Fig. 2 (a) A portion of the 2D sheet structure of **2**. (b) Illustration of the (4,4) network topology in **2** with various metal-to-metal distances. (c) Perspective view of the single 2D layer. (d) Perspective view of the three 2D layers in **2**. The distance between the two adjacent layers is 11.2 Å.

through solid-state PL analysis at room temperature. Fig. S12† displays the UV-vis spectra of solid-state compounds **1** and **2**, with intense absorbance below 240 nm and a shoulder extending to the visible region of the spectrum. As shown in Fig. 3a, upon excitation at 365 nm, compound **1** showed PL emission with a broad emission range of 390–690 nm at ambient temperature in its solid state. The emission maximum for **1** appeared at 530 nm. Compound **2** emits at a rather narrower range of 390–490 nm upon excitation at a wavelength of 365 nm, with an emission maximum at 430 nm, which corresponds to blue emission. The ligand NDA in DMF is known to emit light at an emission maximum of 440 nm upon 365 nm excitation. The emission of NDA is caused by π–π^* and n–π^* transitions.

The PL emission peak maximum of **1** showed a red shift in wavelength to 90 nm in comparison to the ligand. As shown in Fig. 3a, compound **2** showed a higher in PL emission intensity at 440 nm with 365 nm excitation in comparison to the free ligand. In contrast to compound **1**, the PL emission peak maximum of compound **2** was found to be blue shifted by about 8 nm relative to the ligand. The PL emission in both compounds **1** and **2** is attributed to the significant effect of the metal centers, which results in both blue and red shifts in PL emission maxima compared to the free ligand. The PL emission in both compounds is due to the substantial role of the metal ions, which is evident from the time-resolved PL emission spectra shown in Fig. 3b–d. Time-resolved PL emission decays for **1** and **2** can be fitted with three-component exponential decay. PL emission decay for compound **1** at 530 nm exhibits an average excited state lifetime of 8.2 ns, while compound **2** exhibits a shorter average lifetime of 3.1 ns. The longer lifetime of **1** in comparison to **2** is attributed to a distinct PL emission mechanism for **1** that is common in Pb-based materials. This mechanism is often attributed to a more delocalized excited state structure, such as self-trapped excitons. This proposed excited-state structural dynamics of compounds **1** and **2** matched the structural differences seen in crystallographic data.[36,37] Pb-based materials, particularly 2D perovskites, commonly show a WHE mechanism due to self-trapped exciton emission from bulk materials.[38–41] Therefore, owing to the longer emission lifetime and larger Stokes shifts observed for **1**, its PL emission mechanism could be correlated with the analogous PL emission mechanism of Pb-based materials, although further evidence is required to substantiate this proposal. Fig. 4 shows the CIE chromaticity diagram, which shows the emission of measurable colors. According to this diagram, when excited at a wavelength of 365 nm, the chromaticity parameters of **1** are (0.27, 0.34), whereas the values of **2** are (0.17, 0.12), indicating white and blue light emissions, respectively. Compound **1** displays an extremely noticeable emission that is close to the white-light zone, as the chromaticity diagram illustrates. It is difficult to achieve excellent white light emitting material. However, as depicted

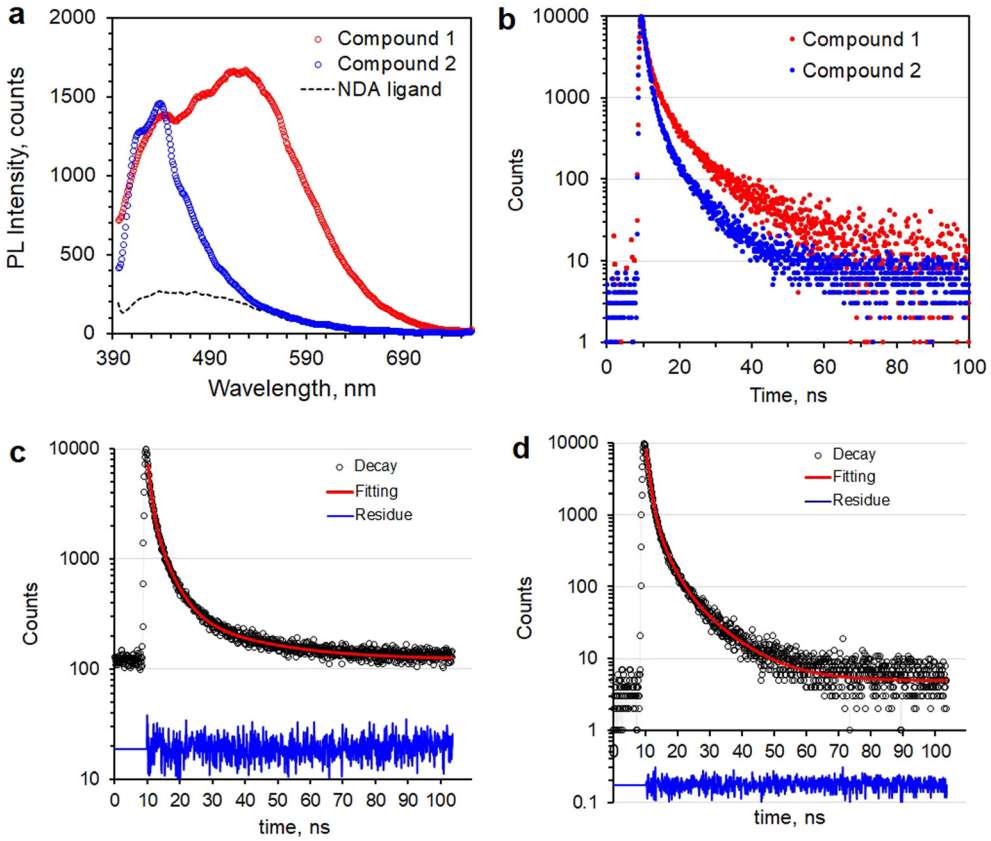

Fig. 3 a) Unnormalized PL spectra for compounds **1** and **2** as well as for NDA in solid state form at ambient temperature upon excitation at 365 nm. b) Comparison of room temperature time-dependent PL emission spectra for compounds **1** and **2**. c) Time-resolved PL emission decay fitting profile for compound **1** at 530 nm upon excitation at 365 nm. d) Time-resolved PL emission decay fitting profile for compound **2** at 430 nm upon excitation at 365 nm.

in Fig. 4, compound **1** has a prominent peak at 570 nm with a red-shifted emission. This emission is highly near pure white, as indicated by the CIE coordinates. Thus, compound **1** has a promising potential for the development of white-light emitting materials.

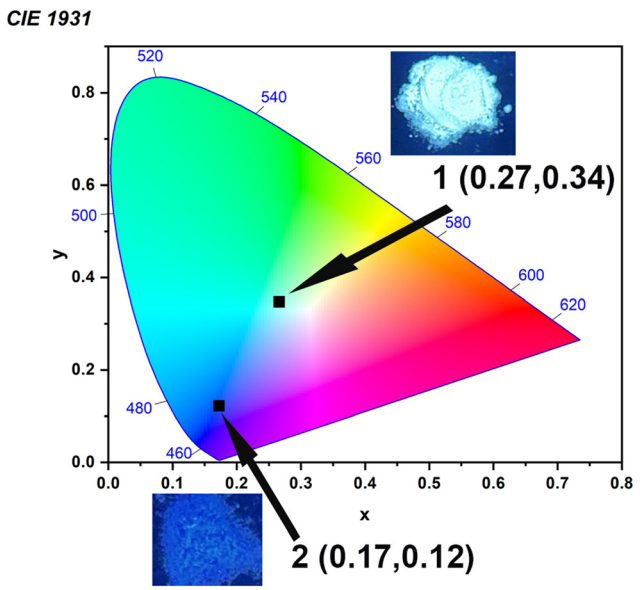

Fig. 4 CIE chromaticity diagram for compounds **1** and **2** (λ_{ex} = 365 nm). The photograph shows the emission of **1** and **2** solids when exposed to light.

Conclusion

Two 2D MOFs were synthesized using NDA as a ligand with Pb(II) and Zn(II) metal ions. The synthesized MOFs display distinct photophysical properties, which are correlated with structural differences seen in the crystallographic data. Both **1** and **2** form 2D sheet-like geometries by chelating and bridging carboxylate ligands of NDA. The interaction of the dicarboxylate ligand in specific stereochemistry results in the formation of two different 2D sheets. Both compounds exhibit PL emission at room temperature in their solid state. In particular, compound **1** emitted near white light, whereas compound **2** emitted blue light. Differences in PL emission properties are attributed to self-trapped exciton emission in compound **1**, which is in agreement with the shifts together with the structural differences in the distances between the 2D sheets and inter-metallic centers. We anticipate that this research will provide new insights into a deeper understanding of the underlying characteristics of MOF structures and for creating more advanced WLE materials.

Data availability

• The data supporting this article have been included as part of the ESI.†

• Crystallographic data for **1** and **2** have been deposited at the CCDC under deposition numbers 2356413 and 2356409, respectively.

Conflicts of interest

There are no conflicts to declare.

Acknowledgements

A. M. P. Peedikakkal would like to acknowledge the support provided by the Deanship of Research Oversight and Coordination (DROC) at King Fahd University of Petroleum and Minerals (KFUPM) for funding this work through project No. DF191031.

References

1 M. Gutiérrez, Y. Zhang and J.-C. Tan, Confinement of luminescent guests in metal–organic frameworks: understanding pathways from synthesis and multimodal characterization to potential applications of LG@MOF systems, *Chem. Rev.*, 2022, **122**, 10438–10483.

2 W. P. Lustig, S. Mukherjee, N. D. Rudd, A. V. Desai, J. Li and S. K. Ghosh, Metal–organic frameworks: functional luminescent and photonic materials for sensing applications, *Chem. Soc. Rev.*, 2017, **46**, 3242–3285.

3 Y. Zhao, H. Zeng, X.-W. Zhu, W. Lu and D. Li, Metal–organic frameworks as photoluminescent biosensing platforms: mechanisms and applications, *Chem. Soc. Rev.*, 2021, **50**, 4484–4513.

4 M. D. Allendorf, C. A. Bauer, R. K. Bhakta and R. J. T. Houk, Luminescent metal–organic frameworks, *Chem. Soc. Rev.*, 2009, **38**, 1330–1352.

5 H. Kaur, S. Sundriyal, V. Pachauri, S. Ingebrandt, K.-H. Kim, A. L. Sharma and A. Deep, Luminescent metal-organic frameworks and their composites: Potential future materials for organic light emitting displays, *Coord. Chem. Rev.*, 2019, **401**, 213077.

6 W. P. Lustig and J. Li, Luminescent metal–organic frameworks and coordination polymers as alternative phosphors for energy efficient lighting devices, *Coord. Chem. Rev.*, 2018, **373**, 116–147.

7 Y. Chen, X. Yin, Z. Chen, P. Wang and B. Li, Tunable White Light Emission of a Metal–Organic Framework Based on a Bisquinoxaline Derivative by Introducing Red–Green Cationic Dyes, *Inorg. Chem.*, 2023, **62**, 10626–10634.

8 C.-Y. Sun, X.-L. Wang, X. Zhang, C. Qin, P. Li, Z.-M. Su, D.-X. Zhu, G.-G. Shan, K.-Z. Shao and H. Wu, Efficient and tunable white-light emission of metal–organic frameworks by iridium-complex encapsulation, *Nat. Commun.*, 2013, **4**, 2717.

9 M.-S. Wang, S.-P. Guo, Y. Li, L.-Z. Cai, J.-P. Zou, G. Xu, W.-W. Zhou, F.-K. Zheng and G.-C. Guo, A direct white-light-emitting metal– organic framework with tunable yellow-to-white photoluminescence by variation of excitation light, *J. Am. Chem. Soc.*, 2009, **131**, 13572–13573.

10 C. Yu, X. Wang, T. Wu, X. Gu, W. Huang, A. M. Kirillov and D. Wu, Color tuning of intrinsic white-light emission in anthracene-linker coordination networks, *Dalton Trans.*, 2020, **49**, 12082–12087.

11 M. Pan, W.-M. Liao, S.-Y. Yin, S.-S. Sun and C.-Y. Su, Single-phase white-light-emitting and photoluminescent color-tuning coordination assemblies, *Chem. Rev.*, 2018, **118**, 8889–8935.

12 J. Miao, Y. Nie, Y. Li, C. Qin, Y. Ren, C. Xu, M. Yan, K. Liu and G. Liu, Single-component solid state white-light emission and photoluminescence color tuning of a Cd (II) complex and its application as a luminescence thermometer, *J. Mater. Chem. C*, 2019, **7**, 13454–13460.

13 Z. Wu, H. Choi and Z. M. Hudson, Achieving White-Light Emission Using Organic Persistent Room Temperature Phosphorescence, *Angew. Chem.*, 2023, **135**, e202301186.

14 X.-D. Wang, Y. Song, W.-Y. Pei and J.-F. Ma, Single-Component White Light Emission from a Metal-Coordinated Cyclotriveratrylene-Based Coordination Polymer, *Inorg. Chem.*, 2022, **61**, 10768–10773.

15 R. Chen, H. Gu, Y. Han, J. Yin, G. Xing and B.-B. Cui, Broadband white-light emission from a novel two-dimensional metal halide assembled by Pb–Cl hendecahedrons, *J. Mater. Chem. C*, 2022, **10**, 9465–9470.

16 M.-Y. Xu, G.-Y. Liang, J.-S. Feng, G.-M. Liang and X.-J. Wang, Temperature-induced structural transformations of lanthanide coordination polymers based on a semirigid tricarboxylic acid ligand: crystal structures and luminescence properties, *Cryst. Growth Des.*, 2022, **22**, 1583–1593.

17 L. Fan, K. Liu, Q. Zeng, M. Li, H. Cai, J. Zhou, S. He, J. Zhao and Q. Liu, Efficiency-tunable single-component white-light emission realized in hybrid halides through metal co-occupation, *ACS Appl. Mater. Interfaces*, 2021, **13**, 29835–29842.

18 G. Chakraborty, I.-H. Park, R. Medishetty and J. J. Vittal, Two-dimensional metal-organic framework materials: synthesis, structures, properties and applications, *Chem. Rev.*, 2021, **121**, 3751–3891.

19 Z. Feng, D. Wang, X. Yang, D. Jin, D. Zhong, B. Liu, G. Zhou, M. Ma and Z. Wu, Asymmetric heteroleptic Ir (III) phosphorescent complexes with aromatic selenide and selenophene groups: Synthesis and photophysical, electrochemical, and electrophosphorescent behaviors, *Inorg. Chem.*, 2018, **57**, 11027–11043.

20 Y. Atoini, L. M. Cavinato, J. Fernandez-Cestau, Y. Gmach, D. Van Opdenbosch and R. D. Costa, From Blue to White: Sustainable Luminescent Metal Organic Framework for Hybrid Light-Emitting Diodes, *Adv. Opt. Mater.*, 2023, **11**, 2202643.

21 A. M. P. Peedikakkal, H. S. Quah, S. Chia, A. S. Jalilov, A. R. Shaikh, H. A. Al-Mohsin, K. Yadava, W. Ji and J. J. Vittal, Near-white light emission from Lead (II) metal–organic frameworks, *Inorg. Chem.*, 2018, **57**, 11341–11348.

22 A. M. P. Peedikakkal, A. S. Jalilov, A. R. Shaikh, A. N. Kalanthoden and A. A. Al-Saadi, Blue-and white-light-emitting 2D-coordination polymers and their solid-state photodimerization reaction, *CrystEngComm*, 2021, **23**, 7663–7670.

23 M. A. A. Al-Nubi, A. M. Hamisu, F. Y. Wardana, A. Ariffin, H. Jo, K. M. Ok and A. C. Wibowo, Lead–organic frameworks containing trimesic acid: facile dissolution–crystallization and near-white light emission, *Cryst. Growth Des.*, 2019, **19**, 6274–6282.

24 Z. Wang, J. Chen, Q. Li, H. Zhang and J. Zhang, Multicolor Fluorescent Lead-MOFs for White-Light-Emitting and Anticounterfeiting Applications, *Adv. Opt. Mater.*, 2023, **11**, 2202743.

25 P. Fu, S. Geng, R. Mi, R. Wu, G. Zheng, B. Su, Z. Xia, G. Niu, J. Tang and Z. Xiao, Achieving Narrowed Bandgaps and Blue-Light Excitability in Zero-Dimensional Hybrid Metal Halide Phosphors via Introducing Cation–Cation Bonding, *Energy Environ. Mater.*, 2024, **7**, e12518.

26 C. Li, Z. Ren, X. Sun, H. Li and S. Yan, Deep-blue thermally activated delayed fluorescence polymers for nondoped solution-processed organic light-emitting diodes, *Macro.*, 2019, **52**, 2296–2303.

27 R. J. Marshall, Y. Kalinovskyy, S. L. Griffin, C. Wilson, B. A. Blight and R. S. Forgan, Functional Versatility of a Series of Zr Metal–Organic Frameworks Probed by Solid-State Photoluminescence Spectroscopy, *J. Am. Chem. Soc.*, 2017, **139**, 6253–6260.

28 S. Yuan, P. Zhang, L. Zhang, A. T. Garcia-Esparza, D. Sokaras, J.-S. Qin, L. Feng, G. S. Day, W. Chen and H. F. Drake, Exposed equatorial positions of metal centers via sequential ligand elimination and installation in MOFs, *J. Am. Chem. Soc.*, 2018, **140**, 10814–10819.

29 L. Y. Xin, G. Z. Liu, L. F. Ma and L. Y. Wang, Coligand-regulated assembly, fluorescence, and magnetic properties of Co(II) and Cd(II) complexes with a non-coplanar dicarboxylate, *J. Solid State Chem.*, 2013, **206**, 233–241.

30 D. A. Alentiev and M. V. Bermeshev, Design and Synthesis of Porous Organic Polymeric Materials from Norbornene Derivatives, *Polym. Rev.*, 2022, **62**, 400–437.

31 D. Yang, Y. Chen, Z. Su, X. Zhang, W. Zhang and K. Srinivas, Organic Carboxylate-Based MOFs and Derivatives for Electrocatalytic Water Oxidation, *Coord. Chem. Rev.*, 2021, **428**, 213619.

32 A. J. Howarth, Y. Liu, P. Li, Z. Li, T. C. Wang, J. T. Hupp and O. K. Farha, Chemical, Thermal and Mechanical Stabilities of Metal–Organic Frameworks, *Nat. Rev. Mater.*, 2016, **1**, 1–15.

33 G. M. Sheldrick, *SADABS, Programs for Scaling and Absorption Correction of Area Detector Data*, University of Göttingen, Göttingen, Germany, 1997.

34 G. M. Sheldrick, *SHELX-97: Programs for Crystal Structure Analysis*, University of Göttingen, Göttingen, Germany, 1997.

35 B. Moulton and M. J. Zaworotko, From molecules to crystal engineering: supramolecular isomerism and polymorphism in network solids, *Chem. Rev.*, 2001, **101**, 1629–1658.

36 Y.-H. Zhao, H.-B. Xu, Y.-M. Fu, K.-Z. Shao, S.-Y. Yang, Z.-M. Su, X.-R. Hao, D.-X. Zhu and E.-B. Wang, A series of lead (II)-organic frameworks based on pyridyl carboxylate acid N-oxide derivatives: syntheses, structures, and luminescent properties, *Cryst. Growth Des.*, 2008, **8**, 3566–3576.

37 J. He, M. Zeller, A. D. Hunter and Z. Xu, White light emission and second harmonic generation from secondary group participation (SGP) in a coordination network, *J. Am. Chem. Soc.*, 2012, **134**, 1553–1559.

38 M. D. Smith and H. I. Karunadasa, White-light emission from layered halide perovskites, *Acc. Chem. Res.*, 2018, **51**, 619–627.

39 L. Lian, P. Zhang, G. Liang, Y. Xia, J. Gao, D. Zhang and J. Zhang, Full-Spectrum White-Light Emission from Triple Self-Trapped Excitons in Hybrid Mixed-Metal Halides, *ACS Appl. Mater. Interfaces*, 2024, **16**, 9030–9038.

40 C. Yang, Q. Wei, Y. Gong, M. Long, G. Zhou, G. Xing and B. Wu, Correlated Self-Trapped Excitons and Free Excitons with Intermediate Exciton–Phonon Coupling in 2D Mixed-Halide Perovskites, *J. Phys. Chem. Lett.*, 2023, **14**, 10046–10053.

41 L. Xiong, H. Sun, S. Li and H. Jiang, First-Principles Investigation on the Stability, Electronic Structure, and Exciton Self-Trapping Mechanism of 0D and 1D $Cs_3Cu_2Cl_5$, *J. Phys. Chem. C*, 2023, **127**, 9113–9120.

